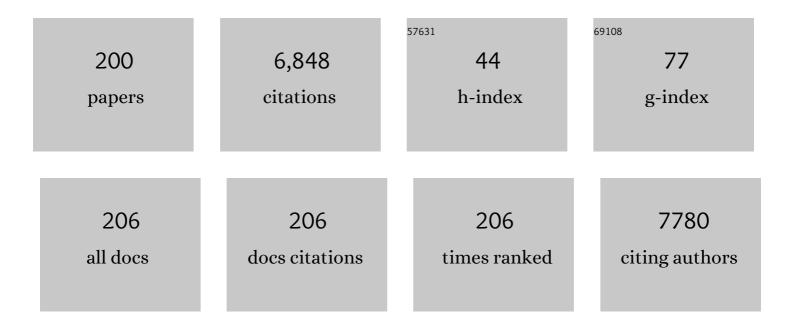
List of Publications by Year in descending order

Source: https://exaly.com/author-pdf/3275225/publications.pdf Version: 2024-02-01



#	Article	IF	CITATIONS
1	Modeling surface spin polarization on ceria-supported Pt nanoparticles. Journal of Physics Condensed Matter, 2022, , .	0.7	0
2	Exploring Blob Detection to Determine Atomic Column Positions and Intensities in Time-Resolved TEM Images with Ultra-Low Signal-to-Noise. Microscopy and Microanalysis, 2022, 28, 1917-1930.	0.2	4
3	Impact of Aliovalent Alkaline-Earth metal solutes on Ceria Grain Boundaries: A density functional theory study. Acta Materialia, 2021, 205, 116481.	3.8	5
4	Atomic Scale Characterization of Fluxional Cation Behavior on Nanoparticle Surfaces: Probing Oxygen Vacancy Creation/Annihilation at Surface Sites. ACS Nano, 2021, 15, 2624-2634.	7.3	21
5	Dynamic structure of active sites in ceria-supported Pt catalysts for the water gas shift reaction. Nature Communications, 2021, 12, 914.	5.8	103
6	Role of Convergence and Collection Angles in the Excitation of Long- and Short-Wavelength Phonons with Vibrational Electron Energy-Loss Spectroscopy. Microscopy and Microanalysis, 2021, 27, 1069-1077.	0.2	8
7	Effect of Cation Point Defects in Doped Ceria Materials on Surface Oxygen Vacancies and Exchange Reactions. Microscopy and Microanalysis, 2021, 27, 2932-2934.	0.2	0
8	An Atomic Level Study of Localized Strain Fields on Multiple Low-Index Ceria (CeO2) Nanoparticle Surfaces. Microscopy and Microanalysis, 2021, 27, 2918-2920.	0.2	0
9	Coupling of Photonic and Plasmonic Modes in Oxide and Supported Metal Nanoparticles: Finite Element Simulation and EELS Study. Microscopy and Microanalysis, 2021, 27, 888-890.	0.2	1
10	Probing Properties of Nanomaterials with Advanced Electron Energy-Loss Spectroscopy. Microscopy and Microanalysis, 2021, 27, 872-874.	0.2	2
11	From In Situ Conversion to Chemical Reaction Kinetics: Development of Truly Operando TEM and its Application to CeO2-Supported Pt Catalysts. Microscopy and Microanalysis, 2021, 27, 2970-2972.	0.2	0
12	Atom Detection in Time-resolved TEM Image Series: Application of Computer Vision Techniques to Noise-degraded Frames. Microscopy and Microanalysis, 2021, 27, 2224-2225.	0.2	1
13	Studying Charge Transport and Light Induced Structural Alterations in Ni/NiO Core-Shell Co-Catalysts on SrTiO3 for Solar Hydrogen Evolution. Microscopy and Microanalysis, 2021, 27, 2982-2984.	0.2	0
14	In-situ TEM Study of Oxygen Surface Exchange on Ceria, Gd-doped Ceria and Pr-doped Ceria. Microscopy and Microanalysis, 2021, 27, 2244-2245.	0.2	0
15	Describing Atomic-Level Fluxional Behavior in Nanoparticles. Microscopy and Microanalysis, 2021, 27, 1306-1307.	0.2	1
16	CrO _x -Mediated Performance Enhancement of Ni/NiO-Mg:SrTiO ₃ in Photocatalytic Water Splitting. ACS Catalysis, 2021, 11, 11049-11058.	5.5	22
17	Developing and Evaluating Deep Neural Network-Based Denoising for Nanoparticle TEM Images with Ultra-Low Signal-to-Noise. Microscopy and Microanalysis, 2021, 27, 1431-1447.	0.2	23
18	Linking Changes in Reaction Kinetics and Atomic-Level Surface Structures on a Supported Ru Catalyst for CO Oxidation. ACS Catalysis, 2021, 11, 1456-1463.	5.5	18

#	Article	IF	CITATIONS
19	In-Plane Structural Fluctuations in Differently Condensed Graphitic Carbon Nitrides. Chemistry of Materials, 2021, 33, 195-204.	3.2	23
20	Atomic level fluxional behavior and activity of CeO2-supported Pt catalysts for CO oxidation. Nature Communications, 2021, 12, 5789.	5.8	53
21	Approaches to Exploring Spatio-Temporal Surface Dynamics in Nanoparticles with <i>In Situ</i> Transmission Electron Microscopy. Microscopy and Microanalysis, 2020, 26, 86-94.	0.2	13
22	Linking Macroscopic and Nanoscopic Ionic Conductivity: A Semiempirical Framework for Characterizing Grain Boundary Conductivity in Polycrystalline Ceramics. ACS Applied Materials & Interfaces, 2020, 12, 507-517.	4.0	14
23	New Data-Driven Interacting-Defect Model Describing Nanoscopic Grain Boundary Compositions in Ceramics. Journal of Physical Chemistry C, 2020, 124, 23619-23625.	1.5	5
24	Chemical kinetics for operando electron microscopy of catalysts: 3D modeling of gas and temperature distributions during catalytic reactions. Ultramicroscopy, 2020, 218, 113080.	0.8	7
25	Properties of Dipole-Mode Vibrational Energy Losses Recorded From a TEM Specimen. Microscopy and Microanalysis, 2020, 26, 1117-1123.	0.2	7
26	Exploring Phononic and Photonic Excitations with Monochromated STEM EELS. Microscopy and Microanalysis, 2020, 26, 1494-1496.	0.2	0
27	Atomic-resolution <i>Operando</i> and Time-resolved <i>In Situ</i> TEM Imaging of Oxygen Transfer Reactions Catalyzed by CeO ₂ -supported Pt Nanoparticles. Microscopy and Microanalysis, 2020, 26, 1694-1695.	0.2	4
28	Tracking the picoscale spatial motion of atomic columns during dynamic structural change. Ultramicroscopy, 2020, 213, 112978.	0.8	19
29	An Open-Cell Environmental Transmission Electron Microscopy Technique for In Situ Characterization of Samples in Aqueous Liquid Solutions. Microscopy and Microanalysis, 2020, 26, 134-138.	0.2	10
30	Towards Chemical Kinetics for Operando Electron Microscopy of Catalysts: 3D Modeling of Product Gas Distributions and Temperature Profiles During Catalysis. Microscopy and Microanalysis, 2020, 26, 2440-2442.	0.2	0
31	Atomic Resolution Vibrational Spectroscopy with On-Axis Detector Geometry. Microscopy and Microanalysis, 2019, 25, 596-597.	0.2	0
32	Nanoscale Probing of Adsorbates on Pt/CeO ₂ with Aloof-beam Vibrational Electron Energy-loss Spectroscopy. Microscopy and Microanalysis, 2019, 25, 644-645.	0.2	2
33	<i>Operando</i> Insight into Oxygen Transfer at Pt/CeO ₂ Interfaces during CO Oxidation. Microscopy and Microanalysis, 2019, 25, 1508-1509.	0.2	2
34	Finite Element Modeling of Gas and Temperature Distributions during Catalytic Reactions in an Environmental Transmission Electron Microscope. Microscopy and Microanalysis, 2019, 25, 2014-2015.	0.2	1
35	Sensing Interfacial Visible Light Absorption in TiO2-supported CeO2â^'x Photocatalyst Nanoparticles. Microscopy and Microanalysis, 2019, 25, 2084-2085.	0.2	0
36	Background Modelling for Quantitative Analysis in Vibrational EELS. Microscopy and Microanalysis, 2019, 25, 674-675.	0.2	4

#	Article	IF	CITATIONS
37	Dynamic Restructuring during Processing: Approaches to Higher Temporal Resolution. Microscopy and Microanalysis, 2019, 25, 1464-1465.	0.2	3
38	Manipulation of Optical Phonon Polaritons in Patterned SiO2 Thin-Films. Microscopy and Microanalysis, 2019, 25, 646-647.	0.2	0
39	Quantifying Structural Transformations from Redox Reactions in TiO2. Microscopy and Microanalysis, 2019, 25, 1476-1477.	0.2	0
40	In Situ Tracking of Picoscale Atomic Displacements with Millisecond Temporal-Resolution During Exchange and Diffusion Processes in Energy Materials in TEM. Microscopy and Microanalysis, 2019, 25, 2004-2005.	0.2	0
41	Structure-Activity Relationships in Pt-Functionalized Graphitic Carbon Nitride Photocatalysts. Microscopy and Microanalysis, 2019, 25, 2202-2203.	0.2	0
42	Probing Local Structures and Disorder in Graphitic Carbon Nitrides. Microscopy and Microanalysis, 2019, 25, 1690-1691.	0.2	1
43	Real-Time Imaging of Surface Dynamics on CeO2 Nanoparticles using Time-Resolved Aberration-Corrected TEM. Microscopy and Microanalysis, 2019, 25, 2050-2051.	0.2	0
44	Vibrational spectroscopy at atomic resolution with electron impact scattering. Nature Physics, 2019, 15, 1237-1241.	6.5	78
45	Nature of the Vibrational-Loss EELS Peaks Measured from Ionic Specimens. Microscopy and Microanalysis, 2019, 25, 618-619.	0.2	0
46	Light induced coarsening of metal nanoparticles. Journal of Materials Chemistry A, 2019, 7, 11756-11763.	5.2	9
47	Nanoscale probing of resonant photonic modes in dielectric nanoparticles with focused electron beams. Physical Review B, 2019, 99, .	1.1	12
48	Oxygen Transfer at Metal-Reducible Oxide Nanocatalyst Interfaces: Contrasting Carbon Growth from Ethane and Ethylene. ACS Applied Nano Materials, 2018, 1, 1360-1369.	2.4	14
49	Photocorrosion of Particles in Aqueous Solutions in an Open Cell in the Environmental Transmission Electron Microscope. Microscopy and Microanalysis, 2018, 24, 290-291.	0.2	0
50	Identification of Rapid Oxygen Exchange Through Site-Dependent Cationic Displacements on CeO2 Nanoparticles. Microscopy and Microanalysis, 2018, 24, 54-55.	0.2	3
51	Oxygen Ion Conductivity and Composition at the Grain Boundaries of Ca Doped CeO2. Microscopy and Microanalysis, 2018, 24, 1540-1541.	0.2	1
52	Importance of Co-catalyst Dispersion in Pt-functionalized Graphitic Carbon Nitride Photocatalysts. Microscopy and Microanalysis, 2018, 24, 1646-1647.	0.2	0
53	Characterization of Mixed Metal Oxide Interfaces Based on TiO2-supported CeO2-x Nanoparticles. Microscopy and Microanalysis, 2018, 24, 458-459.	0.2	0
54	Interpreting Cation Displacements and Image Motifs Associated with the Oxygen Exchange Reaction on CeO2 Nanoparticles. Microscopy and Microanalysis, 2018, 24, 144-145.	0.2	1

#	Article	IF	CITATIONS
55	Probing Functionality for Energy Related Materials; Opportunities for Advanced Electron Microscopy. Microscopy and Microanalysis, 2018, 24, 1468-1469.	0.2	0
56	Determination of Surface Dynamics on CeCh Nanoparticles Using Time-Resolved High-Resolution TEM. Microscopy and Microanalysis, 2018, 24, 1906-1907.	0.2	0
57	Controlled Synthesis of Metal-Support Interface for High Activity CeO2-Supported Pt Nanoparticles. Microscopy and Microanalysis, 2018, 24, 1666-1667.	0.2	0
58	Vibrational electron energy loss spectroscopy in truncated dielectric slabs. Physical Review B, 2018, 98, .	1.1	23
59	Utilizing Aloof-beam Vibrational EELS for the Detection of Hydrogen and Defect Heterogeneity in Carbon Nitrides. Microscopy and Microanalysis, 2018, 24, 426-427.	0.2	0
60	Local Structural Analysis of Graphitic Carbon Nitrides. Microscopy and Microanalysis, 2018, 24, 1990-1991.	0.2	0
61	Atomic-Resolution Operando Observations of Nanostructured Pt/CeC2 Catalysts Performing CO Oxidation. Microscopy and Microanalysis, 2018, 24, 236-237.	0.2	4
62	Atomic Resolution Transmission Electron Microscopy of Perovskite Nanoparticle Surfaces Exposed to Gas Environments at Elevated Temperatures. Microscopy and Microanalysis, 2018, 24, 1488-1489.	0.2	0
63	Dy- and Tb-doped CeO2-Ni cermets for solid oxide fuel cell anodes: electrochemical fabrication, structural characterization, and electrocatalytic performance. Journal of Solid State Electrochemistry, 2018, 22, 3761-3773.	1.2	5
64	Nanoscale Probing of Local Hydrogen Heterogeneity in Disordered Carbon Nitrides with Vibrational Electron Energy-Loss Spectroscopy. ACS Nano, 2018, 12, 5463-5472.	7.3	42
65	The influence of surfaces and interfaces on high spatial resolution vibrational EELS from SiO2. Microscopy (Oxford, England), 2018, 67, i14-i23.	0.7	24
66	Aloof-beam Vibrational Electron Energy-loss Spectroscopy of Adsorbate/Metal Particle Systems. Microscopy and Microanalysis, 2018, 24, 460-461.	0.2	5
67	Al ₂ O ₃ and SiO ₂ Atomic Layer Deposition Layers on ZnO Photoanodes and Degradation Mechanisms. ACS Applied Materials & Interfaces, 2017, 9, 16138-16147.	4.0	26
68	Vibrational and valence aloof beam EELS: A potential tool for nondestructive characterization of nanoparticle surfaces. Ultramicroscopy, 2017, 180, 104-114.	0.8	64
69	Enhanced ionic conductivity in electroceramics by nanoscale enrichment of grain boundaries with high solute concentration. Nanoscale, 2017, 9, 17293-17302.	2.8	36
70	Interfacial Strain Mapping and Chemical Analysis of Strained-Interface Heterostructures by Nanodiffraction and Electron Energy-Loss Spectroscopy. Microscopy and Microanalysis, 2017, 23, 1776-1777.	0.2	0
71	Revealing the Structure of Graphitic Carbon Nitride through Low-Dose TEM using a Direct Electron Detector. Microscopy and Microanalysis, 2017, 23, 1808-1809.	0.2	1
72	In situ Imaging and Spectroscopy of the Carbon Deposition Mechanism on Ni/CeO2 Solid Oxide Fuel Cell Anode Catalyst. Microscopy and Microanalysis, 2017, 23, 914-915.	0.2	1

PETER A CROZIER

#	Article	IF	CITATIONS
73	In situ TEM observations of Oxygen Surface Dynamics in CeO2 Cubes. Microscopy and Microanalysis, 2017, 23, 1994-1995.	0.2	3
74	Atomic-Resolution Characterization of Surface Structures and Metal-Support Interfaces on Nanostructured Pt/CeO2 Catalysts Performing CO Oxidation. Microscopy and Microanalysis, 2017, 23, 966-967.	0.2	1
75	Nanoscale probing of bandgap states on oxide particles using electron energy-loss spectroscopy. Ultramicroscopy, 2017, 178, 2-11.	0.8	9
76	Correlated Electron Microscopy across Length Scales to Elucidate Structural, Electrical and Chemical Properties of Oxide Grain Boundaries. Microscopy and Microanalysis, 2017, 23, 334-335.	0.2	0
77	Local Mapping of Bandgap Electronic State in PrxCe1-xCh2-δ: Elucidating Enhancement and Mechanism of Grain Boundary Electrical Conductivity. Microscopy and Microanalysis, 2017, 23, 1548-1549.	0.2	1
78	Understanding guided light modes in oxide nanoparticles with monochromated EELS. Microscopy and Microanalysis, 2017, 23, 1550-1551.	0.2	0
79	Predicting the Electronic Structure of CeO2 Grain Boundaries for Comparison with Atomic Resolution EELS. Microscopy and Microanalysis, 2017, 23, 1556-1557.	0.2	0
80	Probing Interfacial and Surface Effects with Vibrational Electron Energy Loss Spectroscopy. Microscopy and Microanalysis, 2017, 23, 1562-1563.	0.2	0
81	Monochromated EELS and Optical Spectroscopy of Layered Carbon Nitrides. Microscopy and Microanalysis, 2017, 23, 1566-1567.	0.2	0
82	Surface Dynamics Associated with Redox Processes on TiO2 Nanoparticles. Microscopy and Microanalysis, 2017, 23, 906-907.	0.2	1
83	Investigating the Spatial Resolution of Vibrational Electron Energy-Loss Spectroscopy. Microscopy and Microanalysis, 2016, 22, 992-993.	0.2	1
84	Design and Application of an In Situ Illumination System for an Aberration-corrected Environmental Transmission Electron Microscope. Microscopy and Microanalysis, 2016, 22, 730-731.	0.2	4
85	Bandgap State Mapping via Valence-Loss EELS at Grain Boundaries in Non-Stoichiometric Pr x Ce 1-x O 2-δ. Microscopy and Microanalysis, 2016, 22, 970-971.	0.2	0
86	Measuring bandgap states in individual non-stoichiometric oxide nanoparticles using monochromated STEM EELS: The Praseodymium–ceria case. Ultramicroscopy, 2016, 167, 5-10.	0.8	29
87	Coupling of strain, stress, and oxygen non-stoichiometry in thin film Pr _{0.1} Ce _{0.9} O _{2â^î^} . Nanoscale, 2016, 8, 16499-16510.	2.8	28
88	Current status and future directions for in situ transmission electron microscopy. Ultramicroscopy, 2016, 170, 86-95.	0.8	181
89	Photochemical Reaction Patterns on Heterostructures of ZnO on Periodically Poled Lithium Niobate. ACS Applied Materials & Interfaces, 2016, 8, 26365-26373.	4.0	5
90	Nanocharacterization of Strontium Titanate Thin Films and Oxide-Electrode Interfaces in Resistive Switching Devices. Microscopy and Microanalysis, 2016, 22, 1568-1569.	0.2	0

#	Article	IF	CITATIONS
91	Nanoscale Strain and Composition Mapping in Ionic Thin Film Heterostructures for Resistive Switching Devices. Microscopy and Microanalysis, 2016, 22, 518-519.	0.2	0
92	Exploring Vibrational and Electronic Structure of Carbon Nitride Powders Using Monochromated Electron Energy-Loss Spectroscopy. Microscopy and Microanalysis, 2016, 22, 986-987.	0.2	4
93	In situ TEM Observations of Carbon Deposition on Solid Oxide Fuel Cell Anode Materials. Microscopy and Microanalysis, 2016, 22, 1376-1377.	0.2	0
94	Nanoscale Probing of Bandgap States on Oxide Particles Using Electron Energy-Loss Spectroscopy. Microscopy and Microanalysis, 2016, 22, 972-973.	0.2	0
95	Detection of water and its derivatives on individual nanoparticles using vibrational electron energy-loss spectroscopy. Ultramicroscopy, 2016, 169, 30-36.	0.8	38
96	Atomic-Scale Observations of Catalyst Structures under Reaction Conditions and during Catalysis. Chemical Reviews, 2016, 116, 3487-3539.	23.0	261
97	Exploring the Carbon Deposition Mechanism on Ni/Gd Ceria Catalysts. Microscopy and Microanalysis, 2015, 21, 251-252.	0.2	0
98	Opportunities and Challenges for In-Situ Characterization of Photocatalysts in Environmental TEM. Microscopy and Microanalysis, 2015, 21, 735-736.	0.2	0
99	Nano-level Structure-Reactivity Relationships of Ni-NiO Core-shell Co-catalysts on Ta2O5 for Solar Hydrogen Production. Microscopy and Microanalysis, 2015, 21, 639-640.	0.2	0
100	Bandgaps and Surface Inter-Band States in Photocatalysts with High Energy Resolution EELS. Microscopy and Microanalysis, 2015, 21, 1903-1904.	0.2	1
101	Detection and Characterization of OH Vibrational Modes using High Energy Resolution EELS. Microscopy and Microanalysis, 2015, 21, 1473-1474.	0.2	5
102	Novel sample preparation for operando TEM of catalysts. Ultramicroscopy, 2015, 156, 18-22.	0.8	25
103	Structure–reactivity relationships of Ni–NiO core–shell co-catalysts on Ta2O5 for solar hydrogen production. Applied Catalysis B: Environmental, 2015, 172-173, 58-64.	10.8	39
104	Electrical conductivity and grain boundary composition of Gd-doped and Gd/Pr co-doped ceria. Solid State Ionics, 2015, 272, 9-17.	1.3	89
105	<i>In situ</i> and <i>operando</i> transmission electron microscopy of catalytic materials. MRS Bulletin, 2015, 40, 38-45.	1.7	61
106	Structural Evolution during Photocorrosion of Ni/NiO Core/Shell Cocatalyst on TiO ₂ . Journal of Physical Chemistry C, 2015, 119, 7207-7214.	1.5	61
107	Advanced and In Situ Analytical Methods for Solar Fuel Materials. Topics in Current Chemistry, 2015, 371, 253-324.	4.0	4
108	Vibrational spectroscopy in the electron microscope. Nature, 2014, 514, 209-212.	13.7	568

#	Article	IF	CITATIONS
109	Derivation of Optical Properties of Carbonaceous Aerosols by Monochromated Electron Energy-Loss Spectroscopy. Microscopy and Microanalysis, 2014, 20, 748-759.	0.2	12
110	Dealloying of Noble-Metal Alloy Nanoparticles. Nano Letters, 2014, 14, 2569-2577.	4.5	151
111	Analysis of Catalytic Gas Products Using Electron Energy-Loss Spectroscopy and Residual Gas Analysis for <i>Operando</i> Transmission Electron Microscopy. Microscopy and Microanalysis, 2014, 20, 815-824.	0.2	45
112	Full Optical Properties of Carbonaceous Aerosols by High Energy Monochromated Electron Energy-loss Spectroscopy. Microscopy and Microanalysis, 2014, 20, 188-189.	0.2	1
113	Atomic Level In-situ Characterization of Metal/TiO2 Photocatalysts under Light Irradiation in Water Vapor. Microscopy and Microanalysis, 2014, 20, 460-461.	0.2	0
114	Atomic Level In-situ Characterization of NiO-TiO2 Photocatalysts under Light Irradiation in Water Vapor. Microscopy and Microanalysis, 2014, 20, 1512-1513.	0.2	0
115	Atomic Level In Situ Observation of Surface Amorphization in Anatase Nanocrystals During Light Irradiation in Water Vapor. Nano Letters, 2013, 13, 679-684.	4.5	100
116	Characterization of light-absorbing carbon particles at three altitudes in East Asian outflow by transmission electron microscopy. Atmospheric Chemistry and Physics, 2013, 13, 6359-6371.	1.9	23
117	System for <i>In Situ</i> UV-Visible Illumination of Environmental Transmission Electron Microscopy Samples. Microscopy and Microanalysis, 2013, 19, 461-469.	0.2	39
118	Predicting the optimal dopant concentration in gadolinium doped ceria: a kinetic lattice Monte Carlo approach. Modelling and Simulation in Materials Science and Engineering, 2012, 20, 015004.	0.8	31
119	Stabilized Gold Nanoparticles on Ceria Nanorods by Strong Interfacial Anchoring. Journal of the American Chemical Society, 2012, 134, 20585-20588.	6.6	348
120	Anisotropic Nanocrystal Dissolution Observation by in Situ Transmission Electron Microscopy. Nano Letters, 2012, 12, 5708-5713.	4.5	11
121	Operando Transmission Electron Microscopy: A Technique for Detection of Catalysis Using Electron Energy-Loss Spectroscopy in the Transmission Electron Microscope. ACS Catalysis, 2012, 2, 2395-2402.	5.5	74
122	In situ environmental transmission electron microscopy to determine transformation pathways in supported Ni nanoparticles. Micron, 2012, 43, 1188-1194.	1.1	45
123	Preface. Micron, 2012, 43, 1077.	1.1	1
124	In Situ Synthesis and Nanoscale Evolution of Model Supported Metal Catalysts: Ni on Silica. Journal of Physical Chemistry C, 2012, 116, 11486-11495.	1.5	32
125	Metal-free synthesis of carbon nanotubes filled with calcium silicate. Carbon, 2012, 50, 2666-2669.	5.4	14
126	Direct observation of hydrogen spillover in Ni-loaded Pr-doped ceria. Catalysis Today, 2012, 180, 2-8.	2.2	56

8

#	Article	IF	CITATIONS
127	In search of enhanced electrolyte materials: a case study of doubly doped ceria. Journal of Materials Chemistry, 2011, 21, 18991.	6.7	33
128	Nanocharacterization of Heterogeneous Catalysts by Ex Situ and In Situ STEM. , 2011, , 537-582.		6
129	Mechanical Properties of Titanium Nitride Nanocomposites Produced by Chemical Precursor Synthesis Followed by High-P,T Treatment. Materials, 2011, 4, 1747-1762.	1.3	24
130	Atomic‣cale Observation of the Ni Activation Process for Partial Oxidation of Methane Using Inâ€Situ Environmental TEM. ChemCatChem, 2011, 3, 1051-1059.	1.8	62
131	Effects of stress on phase separation in InxGa1â^'xN/GaN multiple quantum-wells. Acta Materialia, 2011, 59, 3759-3769.	3.8	15
132	A model study on the carburization process of iron-based Fischer–Tropsch catalysts using in situ TEM–EELS. Applied Catalysis B: Environmental, 2011, 102, 521-527.	10.8	40
133	Kinetic lattice Monte Carlo model for oxygen vacancy diffusion in praseodymium doped ceria: Applications to materials design. Journal of Solid State Chemistry, 2011, 184, 811-817.	1.4	53
134	In situ analysis of gas composition by electron energy-loss spectroscopy for environmental transmission electron microscopy. Ultramicroscopy, 2011, 111, 177-185.	0.8	81
135	First-principles Study of Defect Migration in RE-doped Ceria (RE = Pr, Gd). Materials Research Society Symposia Proceedings, 2011, 1311, 15801.	0.1	0
136	A spray drying system for synthesis of rare-earth doped cerium oxide nanoparticles. Chemical Physics Letters, 2010, 495, 280-286.	1.2	26
137	A density functional study of defect migration in gadolinium doped ceria. Physical Chemistry Chemical Physics, 2010, 12, 7904.	1.3	71
138	Oxygen vacancy migration in ceria and Pr-doped ceria: A DFT+U study. Journal of Chemical Physics, 2010, 132, 094104.	1.2	128
139	Nanoscale compositional and structural evolution in ceria zirconia during cyclic redox treatments. Journal of Materials Chemistry, 2010, 20, 7497.	6.7	11
140	In situ preparation of Ni–Cu/TiO2 bimetallic catalysts. Journal of Catalysis, 2009, 262, 73-82.	3.1	80
141	Structural Transformation in Ceria Nanoparticles during Redox Processes. Journal of Physical Chemistry C, 2009, 113, 5700-5704.	1.5	64
142	In situ environmental TEM studies of dynamic changes in cerium-based oxides nanoparticles during redox processes. Ultramicroscopy, 2008, 108, 1432-1440.	0.8	132
143	Measuring the Redox Activity of Individual Catalytic Nanoparticles in Cerium-Based Oxides. Nano Letters, 2008, 8, 962-967.	4.5	79
144	Brown Carbon Spheres in East Asian Outflow and Their Optical Properties. Science, 2008, 321, 833-836.	6.0	432

#	Article	IF	CITATIONS
145	Growth behavior near the ultimate resolution of nanometer-scale focused electron beam-induced deposition. Nanotechnology, 2008, 19, 225305.	1.3	46
146	Proximity effects in nanoscale patterning with high resolution electron beam induced deposition. Journal of Vacuum Science & Technology B, 2008, 26, 249.	1.3	12
147	Nanoscale Oxide Patterning with Electronâ 'Solidâ 'Gas Reactions. Nano Letters, 2007, 7, 2395-2398.	4.5	13
148	Nanoscale Heterogeneity in Ceria Zirconia with Low-Temperature Redox Properties. Journal of Physical Chemistry B, 2006, 110, 18278-18285.	1.2	44
149	In situ synthesis and characterization of Ru promoted Co/Al2O3 Fischer–Tropsch catalysts. Applied Catalysis A: General, 2006, 307, 212-221.	2.2	68
150	One nanometer structure fabrication using electron beam induced deposition. Microelectronic Engineering, 2006, 83, 1468-1470.	1.1	24
151	Dynamic nucleation and growth of Ni nanoparticles on high-surface area titania. Surface Science, 2006, 600, 693-702.	0.8	35
152	Beam-Induced Damage to Thin Specimens in an Intense Electron Probe. Microscopy and Microanalysis, 2006, 12, 65-71.	0.2	100
153	Epitaxial semimetallic HfxZr1â^'xB2 templates for optoelectronic integration on silicon. Applied Physics Letters, 2006, 89, 242110.	1.5	11
154	Metal sintering mechanisms and regeneration of palladium/alumina hydrogenation catalysts. Applied Catalysis A: General, 2005, 282, 111-121.	2.2	100
155	Environmental Transmission Electron Microscopy in Nanotechnology. , 2005, , 531-565.		23
156	Atomic-Scale Study of in Situ Metal Nanoparticle Synthesis in a Ni/TiO2System. Journal of Physical Chemistry B, 2005, 109, 13883-13890.	1.2	26
157	Theoretical study of environmental dependence of oxygen vacancy formation in CeO2. Applied Physics Letters, 2005, 87, 141917.	1.5	56
158	Approaching the Resolution Limit of Nanometer-Scale Electron Beam-Induced Deposition. Nano Letters, 2005, 5, 1303-1307.	4.5	251
159	Atomic-scale imaging of asymmetric Lomer dislocation cores at the Ge/Si(001) heterointerface. Applied Physics Letters, 2004, 84, 2530-2532.	1.5	29
160	Synthesis of uniform GaN quantum dot arrays via electron nanolithography of D2GaN3. Applied Physics Letters, 2004, 84, 3441-3443.	1.5	65
161	Synthesis of Uniform GaN Quantum Dot Arrays via Electron Nanolithography of D ₂ GaN ₃ . Microscopy and Microanalysis, 2004, 10, 356-357.	0.2	2
162	In SituElectron Microscopy Studies of the Sintering of Palladium Nanoparticles on Alumina during Catalyst Regeneration Processes. Microscopy and Microanalysis, 2004, 10, 77-85.	0.2	39

#	Article	IF	CITATIONS
163	Determination of Elemental Composition and Structure of Individual Organic Cloud Condensation Nuclei. Microscopy and Microanalysis, 2004, 10, 878-879.	0.2	1
164	Novel Synthetic Pathways to Wide Bandgap Semiconductors in the Si—C—Al—N System ChemInform, 2003, 34, no.	0.1	0
165	Synthesis of Highly Coherent SiGe and Si4Ge Nanostructures by Molecular Beam Epitaxy of H3SiGeH3 and Ge(SiH3)4 ChemInform, 2003, 34, no.	0.1	Ο
166	Microstructural evolution of Ge/Si(100) nanoscale islands. Journal of Crystal Growth, 2003, 259, 232-244.	0.7	34
167	Lattice measurement and alloy compositions in metal and bimetallic nanoparticles. Ultramicroscopy, 2003, 98, 63-72.	0.8	55
168	Stoichiometric and non-stoichiometric films in the Si–O–N system: mechanical, electrical, and dielectric properties. Materials Science and Engineering B: Solid-State Materials for Advanced Technology, 2003, 97, 54-58.	1.7	23
169	Synthesis of Highly Coherent SiGe and Si4Ge Nanostructures by Molecular Beam Epitaxy of H3SiGeH3and Ge(SiH3)4. Chemistry of Materials, 2003, 15, 3569-3572.	3.2	11
170	Nanometer-scale composition measurements of Ge/Si(100) islands. Applied Physics Letters, 2003, 82, 1473-1475.	1.5	77
171	Synthesis of ternary SiGeSn semiconductors on Si(100) via SnxGe1â^'x buffer layers. Applied Physics Letters, 2003, 83, 2163-2165.	1.5	97
172	SnGe superstructure materials for Si-based infrared optoelectronics. Applied Physics Letters, 2003, 83, 3489-3491.	1.5	42
173	Epitaxial growth of group III nitrides on silicon substrates via a reflective lattice-matched zirconium diboride buffer layer. Applied Physics Letters, 2003, 82, 2398-2400.	1.5	56
174	New Magnetic Order in Buried Native Iron Oxide Layers. Physical Review Letters, 2003, 91, 267201.	2.9	28
175	An Environmental Transmission Electron Microscope for In-Situ Observation of Chemical Processes at the Nanometer Level. Microscopy and Microanalysis, 2003, 9, 912-913.	0.2	18
176	Low-Temperature Epitaxial Growth of the Quaternary Wide Band Gap Semiconductor SiCAIN. Physical Review Letters, 2002, 88, 206102.	2.9	36
177	In siturealâ€ŧime environmental TEM of gas phase Ziegler–Natta catalytic polymerization of propylene. Journal of Electron Microscopy, 2002, 51, S27-S39.	0.9	21
178	Evolution of Ge/Si(100) island morphology at high temperature. Applied Physics Letters, 2002, 80, 3623-3625.	1.5	28
179	Novel synthetic pathways to wide bandgap semiconductors in the Si–C–Al–N system. Solid State Sciences, 2002, 4, 1509-1519.	1.5	19
180	Low-temperature growth of SiCAIN films of high hardness on Si(111) substrates. Applied Physics Letters, 2001, 79, 2880-2882.	1.5	16

#	Article	lF	CITATIONS
181	In-Situ and Ex-Situ Microscopic Study of Gas Phase Propylene Polymerization over a High Activity TiCl4-MgCl2 Heterogeneous Ziegler-Natta Catalyst. Macromolecular Rapid Communications, 2001, 22, 34-40.	2.0	25
182	Direct quantitative measurement of compositional enrichment and variations in InyGa1â^'yAs quantum dots. Applied Physics Letters, 2001, 79, 3170-3172.	1.5	19
183	Direct observation of reduction of PdO to Pd metal by in situ electron microscopy. Studies in Surface Science and Catalysis, 2000, 130, 3119-3124.	1.5	16
184	Growth and characterization of CdTe/Si heterostructures — effect of substrate orientation. Materials Science and Engineering B: Solid-State Materials for Advanced Technology, 2000, 77, 93-100.	1.7	40
185	Direct Imaging of Zirconia Pillars in Montmorillonite by Analytical Electron Microscopy. Clays and Clay Minerals, 1999, 47, 683-687.	0.6	2
186	Synthesis, Structure, and Physicochemical and Catalytic Characterization of the Novel High-Silica Large-Pore Zeolite SSZ-42. Chemistry - A European Journal, 1998, 4, 1312-1323.	1.7	49
187	Characterization and application of supported metal catalysts with well-tailored pore systems and metal dispersions. Fresenius' Journal of Analytical Chemistry, 1998, 361, 677-679.	1.5	5
188	Oxidation and Reduction of Small Palladium Particles on Silica. Microscopy and Microanalysis, 1998, 4, 278-285.	0.2	37
189	Quantitative elemental mapping of materials by energy-filtered imaging. Ultramicroscopy, 1995, 58, 157-174.	0.8	93
190	Physicochemical Characterization of Zeolites SSZ-26 and SSZ-33. The Journal of Physical Chemistry, 1994, 98, 12040-12052.	2.9	70
191	Quantitative imaging and diffraction of zeolites using a slow-scan CCD camera. Ultramicroscopy, 1993, 52, 487-498.	0.8	40
192	Low-dose high-resolution electron microscopy of zeolite materials with a slow-scan CCD camera. Ultramicroscopy, 1993, 48, 332-340.	0.8	50
193	Ca segregation and step modifications on cleaved and annealed MgO(100) surfaces. Surface Science, 1993, 284, 186-199.	0.8	27
194	SSZ-26 and SSZ-33: Two Molecular Sieves with Intersecting 10- and 12-Ring Pores. Science, 1993, 262, 1543-1546.	6.0	165
195	Preparation and characterization of MgO surfaces by reflection electron microscopy. Microscopy Research and Technique, 1992, 20, 426-438.	1.2	22
196	Electron-beam-induced reactions at transition-metal oxide surfaces. Vacuum, 1991, 42, 301-308.	1.6	59
197	Measurement of inelastic electron scattering cross-sections by electron energy-loss spectroscopy. The Philosophical Magazine: Physics of Condensed Matter B, Statistical Mechanics, Electronic, Optical and Magnetic Properties, 1990, 61, 311-336.	0.6	43
198	Observation of exit surface sputtering in TiO2 using biased secondary electron imaging. Surface Science, 1990, 237, 232-240.	0.8	30

#	Article	IF	CITATIONS
199	Biassed secondary electron imaging in a UHV-STEM. Ultramicroscopy, 1989, 31, 111-115.	0.8	64
200	A compact parallelâ€recording detector for EELS. Journal of Microscopy, 1987, 148, 157-166.	0.8	19